Camera Modelling with Image-variant Parameters and Finite Elements

Werner Tecklenburg, Thomas Luhmann, Heidi Hastedt
Institute for Applied Photogrammetry and Geoinformatics
University of Applied Sciences Oldenburg/Ostfriesland/Wilhelmshaven
Ofener Str. 16, D-26121 Oldenburg
www.fh-oldenburg.de/iapg

Abstract: Digital high-resolution consumer cameras are widely available, and are increasingly used in close-range photogrammetry. The mechanical construction of the cameras often do not meet photogrammetric requirements, thus they have to be modelled sufficiently. An approach for camera modelling is discussed that introduces image-variant parameters of interior orientation. In addition a correction model based on finite elements is integrated that provides the correction of remaining errors in the sensor space (e.g. unflatness). All functional parameters are estimated simultaneously in a bundle adjustment. Significant improvements of object accuracy have been achieved with respect to standard calibration techniques based on self-calibrating bundle adjustment.

Key words: Camera calibration, finite elements, image-variant interior orientation, distortion, accuracy

1. Introduction

As state-of-the-art usually high-quality digital cameras are used for photogrammetric industrial metrology. The image measurement of points is performed by operators that provide measuring accuracies of 0.03 pixel or even less. This corresponds to an accuracy in image space of 0.25µm or better (Luhmann 2000).

Besides the definition of the object coordinate system by scale and datum definition, the quality of point determination in object space is significantly affected by the model and calibration method of the used camera. By default, most camera models include the principal distance (c_k), principal point (x_h,y_h), radial-symmetric lens distortion (a_1,a_2,a_3), decentring of lenses by tangential and asymmetric distortion (b_1,b_2) and global sensor properties such as affinity and sheering (c_1,c_2). For special cases functional models for deformations of the film or sensor plane have been used (e.g. CAP, BINGO) (Brown 1976, Jacobsen 1980, Kruck 1983). Munji (1986) reports on the application of finite elements for the determination of local imaging errors of partial-metric cameras.

However, it can not be assumed that camera parameters remain stable over the whole period of image acquisition. This is true especially for free hand-held camera shots as they are affected by different mechanical influences by the user. On the one hand gravity effects change with different viewing directions, on the other hand holding the camera can yield to varying strains of the camera body. In the following investigation these effects are considered by the use of image-variant parameters of interior orientation.

In addition the unflatness of the sensor surface shall be taken into account. The type of unflatness could not be predicted a priori as they can be caused by the manufacturing processes of the sensor itself, or by the mounting principle inside the camera body. Consequently, no specialised functional model has been chosen but a grid-based correction model based on finite elements (Fig. 1). The anchor points are distributed raster-wise over the sensor surface with an a priori defined grid width.

Fig. 1: Principle of the correction grid applied for a digital camera (Kodak DCS)

2. Mathematical Model of Camera Parameters

a) Image-variant parameters

Usually camera parameters of interior orientation are applied globally, i.e. identical for all images of a photogrammetric project. Distortion parameters are normally defined with respect to the principal point. Then the standard observation equation yield

$$x' = x'_0 - c \cdot \frac{r_{11} \cdot (X_p - X_0) + r_{21} \cdot (Y_p - Y_0) + r_{31} \cdot (Z_p - Z_0)}{r_{13} \cdot (X_p - X_0) + r_{23} \cdot (Y_p - Y_0) + r_{33} \cdot (Z_p - Z_0)} + dx'$$

$$y' = y'_0 - c \cdot \frac{r_{12} \cdot (X_p - X_0) + r_{22} \cdot (Y_p - Y_0) + r_{32} \cdot (Z_p - Z_0)}{r_{13} \cdot (X_p - X_0) + r_{23} \cdot (Y_p - Y_0) + r_{33} \cdot (Z_p - Z_0)} + dy'$$

Using image-variant parameters another three parameters per image are introduced that describe variations of the principal distance and the shift of the principal point. As a major result the possible displacement and rotation of the lens with respect to the image sensor are compensated by this approach. The extended observation equations yield

$$x' = (x'_0 + \Delta x'_i) - (c + \Delta c_i) \cdot \frac{r_{11} \cdot (X_p - X_0) + r_{21} \cdot (Y_p - Y_0) + r_{31} \cdot (Z_p - Z_0)}{r_{13} \cdot (X_p - X_0) + r_{23} \cdot (Y_p - Y_0) + r_{33} \cdot (Z_p - Z_0)} + dx'_{\langle \ldots\ldots \Delta c_i, \Delta x'_i, \Delta y'_i \rangle}$$

$$y' = (y'_0 + \Delta y'_i) - (c + \Delta c_i) \cdot \frac{r_{12} \cdot (X_p - X_0) + r_{22} \cdot (Y_p - Y_0) + r_{32} \cdot (Z_p - Z_0)}{r_{13} \cdot (X_p - X_0) + r_{23} \cdot (Y_p - Y_0) + r_{33} \cdot (Z_p - Z_0)} + dy'_{\langle \ldots\ldots \Delta c_i, \Delta x'_i, \Delta y'_i \rangle}$$

$$i = 1, \text{number of images}$$

The exterior orientation of an image is extended by these three parameters, hence the number of unknowns grows to nine parameters per image.

It has to be considered that a variation of the principal distance affects lens distortion with respect to the image plane. Consequently, in contrast to standard approaches this effect can

no longer be modelled as a function of image coordinates, but as a function of imaging angle. In addition an image-variant local shift of the principal point also influences the effect of distortion in image plane.

The expected variations of principal distance and principal points are estimated in the range of a few hundreds of a millimetre. Hence, these parameters can be introduced as observed unknowns into the adjustment process weighted according to the a priori accuracy. This approach is most advantageous as adjustment results do not become too "weak", and smearing effects by possible correlations between other adjustment parameters, mostly to the spatial position of the perspective centre, can be avoided.

b.) Finite elements correction model

In order to consider image-invariant parameters the finite elements method has been chosen that uses a raster-type correction grid based on anchor points. Each grid point will provide corresponding correction values in form of plane vectors.

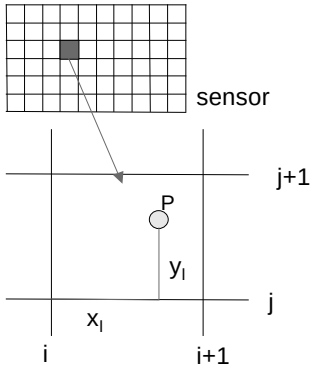

Fig. 2: Interpolation within the correction grid

Correction values for a measured image point are interpolated according to the following linear equation (Kraus 2000; see Fig. 2):

$$\begin{aligned} x_{korr} = (1 - x_l - y_l + x_l \cdot y_l) \cdot k_{x[i,j]} \\ + (x_l - x_l \cdot y_l) \cdot k_{x[i+1,j]} \\ + (y_l - x_l \cdot y_l) \cdot k_{x[i,j+1]} \\ + x_l \cdot y_l \cdot k_{x[i+1,j+1]} \end{aligned}$$

(similar function for y_{korr})

where x_{korr} denotes the correction of the measured image coordinate (x), the coordinates x_l,y_l describe the local position of the measured image point inside the grid element and the elements $k_x[i,j]$, $k_x[i+1,j]$, $k_x[i,j+1]$, $k_x[i+1,j+1]$ identify the participating grid points. In analogy the similar equation results for the image coordinate (y). The collinearity equations are extended by the above described terms.

In order to separate the "signal" from "noise", i.e. separating random measuring errors from the real sensor deformations and not considered imaging errors of the lens, curvature constraints of the correction grid are introduced as pseudo observations (Kraus 2000).

$$\begin{aligned} 0 &= (k_{x[i,j-1]} - k_{x[i,j]}) - (k_{x[i,j]} - k_{x[i,j+1]}) \\ 0 &= (k_{x[i-1,j]} - k_{x[i,j]}) - (k_{x[i,j]} - k_{x[i+1,j]}) \end{aligned}$$

(similar function for $k_{y[\ ]}$)

The equations are applied inside the correction grid in horizontal and in vertical direction as well. This leads to a new group of observations within the equation system. The additional equations are introduced with an appropriate accuracy (weight) that depends on the "roughness" of the estimated unflatness of the correction grid, and of the actual number of measured image points of a particular grid element within the complete set of images.

In addition these equation avoid possible singularities of the adjustment system as they might occur for grid segments without measured image points.

c) Observation weights of individual observation groups

Up to the current stage of investigations the a priori observation weights of image-variant parameters are estimated globally based on the used camera.

In the same way the curvature constraints of the finite element parameters are defined. In addition the dimension of the correction grid has to be considered, i.e. the expected variation of curvature is reduced with increasing density of the correction grid.

3. Results

Within the scope of the analysis concerning the described modelling type for camera calibration a mobile testfield (Fig. 3) with authorization of CERN's survey group was used.

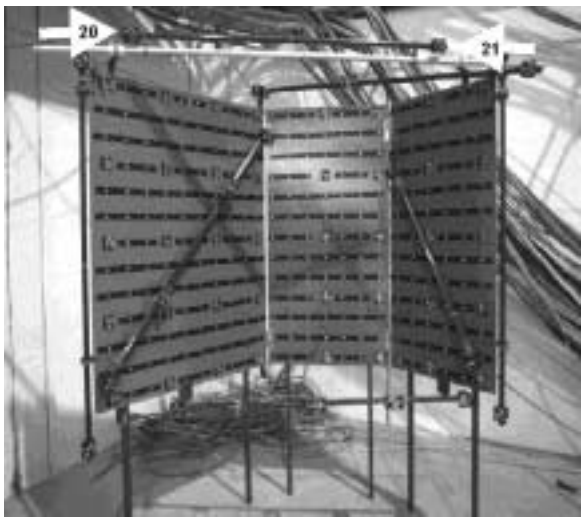

Fig. 3: Mobile testfield (CERN)

This data set includes 59 object points in 35 images whereof 10 are rolled through the camera axis. The images are taken frontal (Fig. 4) with a Kodak DCS 460 digital camera equipped with a 20mm lens. The object includes 7 scalebars whereof 1 is taken for scale definition of the adjustment. Fig. 4 shows the camera stations with reference to the object.

Due to the construction of the used camera (the sensor is attached to only one screw) high residuals regarding image-variant parameters are expected. Additionally the present data set is analysed with bundle adjustment programs (CAP, CDW/DPAwin, Ax.Ori) which base the adjustment on conventional functional camera parameters such as principal distance, principal point, radial-symmetric lens distortion, decentring of lenses by tangential and asymmetric distortion as well as affinity and sheering effects in the image.

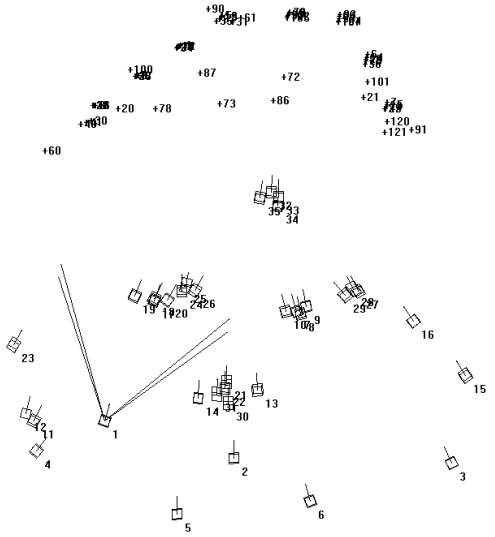

Fig. 4 Topview of object points and camera stations

Compared to the conventional computation the a posteriori accuracy of image measurements increased from 0.4µm up to 0.15µm. Fig. 5 illustrates the results of the method with image-variant parameters. At this the instability of the DCS 460 is obvious, particularly within the tilted images 26-35. The principal point shifts in a range of 40µm. As already shown in (Tecklenburg & Luhmann 2000) an influence of gravity to the camera construction is indicated by the image-variant parameters of the tilted images.

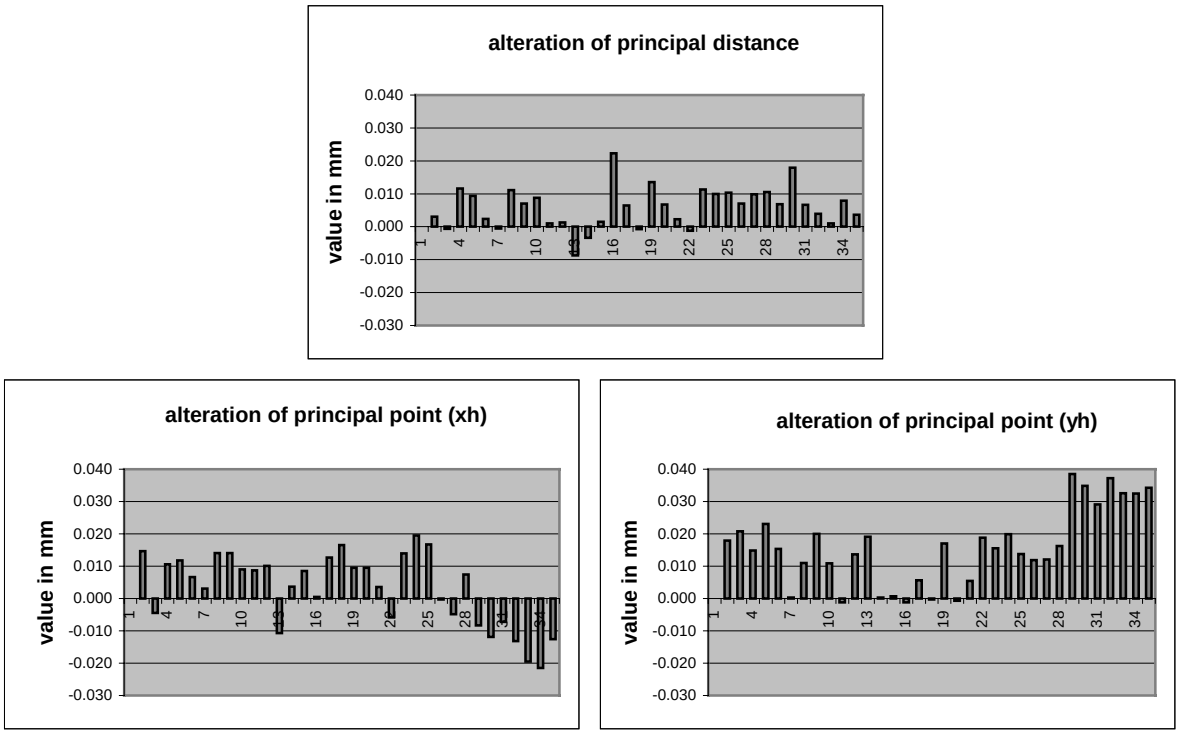

Fig. 5 Alteration of interior orientation – image-variant parameters

For the following evaluation with image-variant parameters and a grid-based correction model an a priori observation accuracy of 1µm for curvature constraints and 5µm for stability of interior orientation is introduced. A correction grid of 9x13 elements was chosen; it corresponds to a raster-width of 2.35mm. The representation of the results (Fig. 6; dark grey grid shows the result indicates extrapolation effects in regions of low object point density (shown in Fig 6 in bright grey). Tangential-asymmetric distortion of the lens is obviously visible in the bottom left and top right corner of the image.

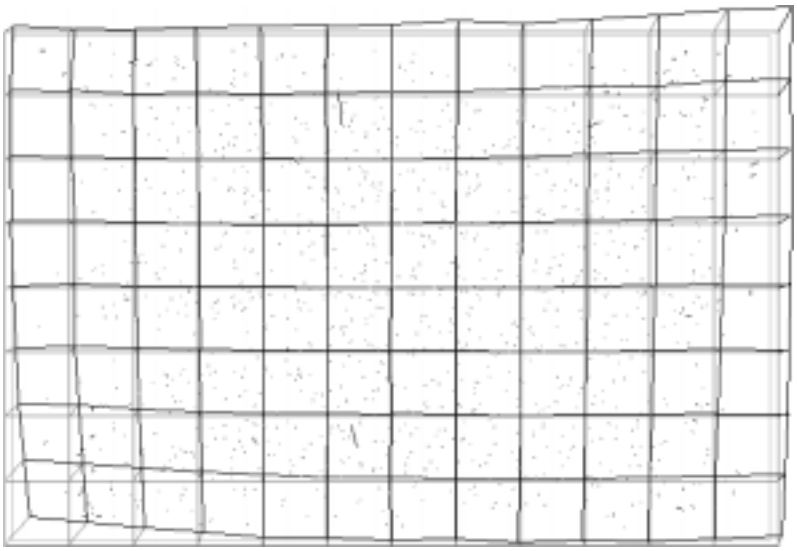

Fig. 6 Finite elements correction grid after adjustment

For comparison of the reached residuals the data set was additionally calculated with CAP, CDW/DPAwin and Ax.Ori (Table 1). For this purpose the scalebar 1 (20-21, shown in Fig. 3) was used for scale definition of the adjustment. Considerable enhancement of accuracy (Fig. 7) from about 0.06mm up to 0.5mm absolute improvement is brought through the method of image-variant parameters combined with a grid-based correction model compared to the conventional mathematical approach.

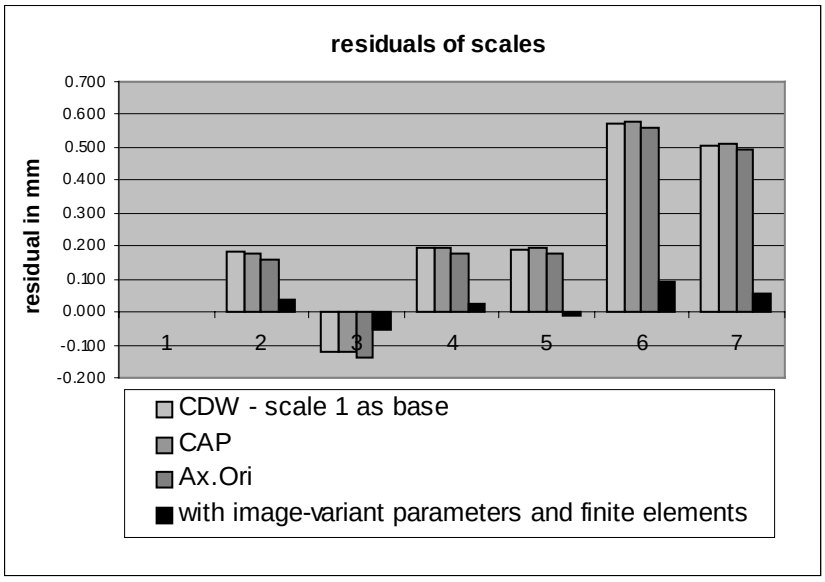

Fig. 7 Residuals of scales in comparison of different adjustments

		CDW/DPAwin	CAP	Ax.Ori	with image-variant parameters and finite elements
RMS of object points (X)	mm	0.01762	0.01749	0.02109	0.01006
RMS of object points (Y)	mm	0.02888	0.02887	0.02949	0.01053
RMS of object points (Z)	mm	0.01436	0.01478	0.01800	0.00834
accuracy of					
image measurements	µm	0.4312	0.4286	0.4490	0.1500
principle distance	mm	20.1538	20.1543	20.1543	20.1394
principle point (xh)	mm	0.1321	0.1325	0.1325	0.1277
principle point (yh)	mm	0.1224	0.1227	0.1226	0.0980
rad.-sym. distortion (a1)		-2.86E-04	-2.86E-04	-2.86E-04	-2.84E-04
rad.-sym. distortion (a2)		6.27E-07	6.30E-07	6.30E-07	6.23E-07
rad.-sym. distortion (a3)		-3.22E-10	-3.34E-10	-3.34E-10	-3.58E-10
residuals in scales					
(shown in Fig. 7)					
scale 1 (20-21) base	mm	0.0000	0.0000	0.0000	0.0000
scale 2 (30-31)	mm	0.1847	0.1798	0.1608	0.0355
scale 3 (40-41)	mm	-0.1203	-0.1181	-0.1365	-0.0540
scale 4 (60-61)	mm	0.1933	0.1966	0.1773	0.0264
scale 5 (90-91)	mm	0.1889	0.1934	0.1753	-0.0105
scale 6 (100-101)	mm	0.5747	0.5793	0.5600	0.0890
scale 7 (120-121)	mm	0.5062	0.5109	0.4924	0.0570

Table 1: Comparison of results

4. Outlook

It can be assumed that the camera parameters calculated by the finite element correction grid can be used again without being recalculated for a new photogrammetric measurement task if they describe stable physical properties of the sensor surface. Hence this approach revives the "old" idea of the metric camera. Within the bundle adjustment only image-variant parameters have to be determined. It can be expected that our approach is more robust against deformations of the object coordinate system, thus yielding results of higher quality. However, the remaining deviations in scales (Fig. 7) let assume that the camera parameters have not been modelled completely yet. The deviations diminished in value but they still point to the same direction. As an example, future investigations have to proof if the principal

point is identical to the intersection point of the optical axis with respect to the image plane. In addition, sensor characteristics are still not separated from the imaging properties of the lens because recently the lens-based parameters include radial-symmetric distortion only. In order to investigate deviations in scale measurements more detailed a testfield configuration according to the new German guideline for acceptance and reverification test of optical 3-D measuring systems will be established (Luhmann & Wendt 2000).

5. References

Brown, D.C. (1976): The bundle adjustment – progress and prospectives. International Archives of Photogrammetry, 21 (3), ISP Congress, Helsinki, pp. 1-33.

Jacobsen, K. (1980): Vorschläge zur Konzeption und zur Bearbeitung von Bündelblock-ausgleichungen. Dissertation, University of Hanover.

Kraus, K. (200): Photogrammetrie, Band 3, Topographische Informationssysteme, Dümmler Verlag, Bonn, p. 188ff.

Kruck, E. (1983): Lösung großer Gleichungssysteme für photogrammetrische Blockausgleichungen mit erweitertem funktionalem Modell. Dissertation, Wiss. Arbeiten der Fachrichtung Vermessungswesen der Universität Hannover, Nr. 128.

Luhmann, T. (2000): Nahbereichsphotogrammetrie. Wichmann Verlag, Heidelberg.

Luhmann, T., Wendt, K. (2000): Recommendations for an Acceptance and Verification Test of Optical 3-D Measurement Systems. International Archives for Photogrammetry and Remote Sensing, Vol. 33/5, p. 493-499, Amsterdam.

Maas, H.-G. (1999): Ein Ansatz zur Selbstkalibrierung von Kameras mit instabiler innerer Orientierung. Publikationen der DGPF, Band 7, München 1998.

Munji, R.A.H. (1986): Self-calibration using the finite element approach. Photogrammetric Engineering and Remote Sensing, Vol. 52, No. 3, March 1986, pp. 411-418.

Munji, R.A.H. (1986): Calibrating non-metric cameras using the finite element method. Photogrammetric Engineering and Remote Sensing, Vol. 52, No. 8, August 1986, pp. 1201-1205.

Tecklenburg, W., Luhmann, T. (2000): Kameramodellierung mit bildvarianten Parametern und Finiten Elementen. Publikationen der DGPF, Band 9.